

Chapter 6

EXPERIMENTATION

6.1. INTRODUCTION

The CFD simulation results which are discussed in the preceding chapters are authenticated with the experimental findings. The experimental study is divided into two sections. In the first section, comparative study of the removal rate using the cylindrical and slotted tool is discussed. In the second section, the high-speed camera images of the flow-field in the IEG is presented. The suitability of the slotted tool for μ ED-milling is found by calculating the MRR and TWR. The effect of different size and shape of the slots on the removal rate is investigated. The experimental method to verify the simulation result is a tedious task due to the micro dimensions of the domain under study. Hence, different methods are utilized for validation depending upon the suitability.

To capture the in-process images of the μ ED-milling process, high-speed video camera is used. The images and videos are taken at a higher frame rate to capture the spark, dielectric and debris flow in the IEG. These cameras are specifically used to study the event occurring at a very high speed. As the field of view is very small and the process being submerged under dielectric fluid, high magnification lenses with the special camera mounting arrangement is used. To visualize the micro and nano size debris particles ejecting from the crater, high magnification microscopic lens is required which are very expensive. Due to this constraint, the existing facility was unable to capture the images of the debris particles. In addition to this, the mounting of lens close to the machining zone was a difficult task due to the presence of tool, workpiece and dielectric tank which increases the working distance between the lens and the field of view. The SEM images at different resolution and magnification are obtained at different locations of machining. The SEM images are used to obtain information regarding debris size, channel shapes, tool shapes and redeposition. The experiments on slotted tool are performed on Hyper-15

μ EDM machine and the experiments to capture high-speed images are performed on hybrid μ EDM machine DT-110. The images are captured using two different setups with two different high-speed cameras.

6.2. SLOTTED TOOL

6.2.1. Experimental setup

The experiments are performed on a Hyper-15 micromachining machine. The experimental setup with all details is shown in Figure 6.1 and the parameters are given in Table 6.1. The tool is mounted rigidly on the spindle using the collet to avoid wobbling during rotation. The workpiece is clamped on the machine table using a fixture. Necessary care is taken to ensure the top surface of the workpiece to be horizontal. The workpiece is EN31 die steel material with a thickness of 4 mm. EN31 is a high carbon alloy steel with a hardness of 63 HRC and the tensile strength of 215000 N/mm². The dielectric is conventional EDM oil and is supplied through a nozzle to ensure continuous recirculation of the fluid. The main aim is to investigate the effect of peripheral slots on ED milling of slots in microdomain. However, with the present manufacturing scenario, it is difficult to cut straight slots on the periphery of cylindrical tools with a diameter below 1 mm. Hence, a tool with a diameter of 2 mm is used for experimentation and the CFD simulation is carried out to study the flow-field in the gap. As the productivity of machining is greatly influenced by MRR and TWR, these are the output responses for the present study.

The MRR and TWR is given as

$$MRR = \frac{V_w}{t} \quad \text{and} \quad TWR = \frac{V_T}{t} \quad (6.1)$$

where V_w is the volume of material removed from the workpiece, V_T is the volume of tool wear and t is the machining time. The comparative study of the cylindrical and slotted tool is done with respect to MRR, TWR and surface topography of the machined work surface.

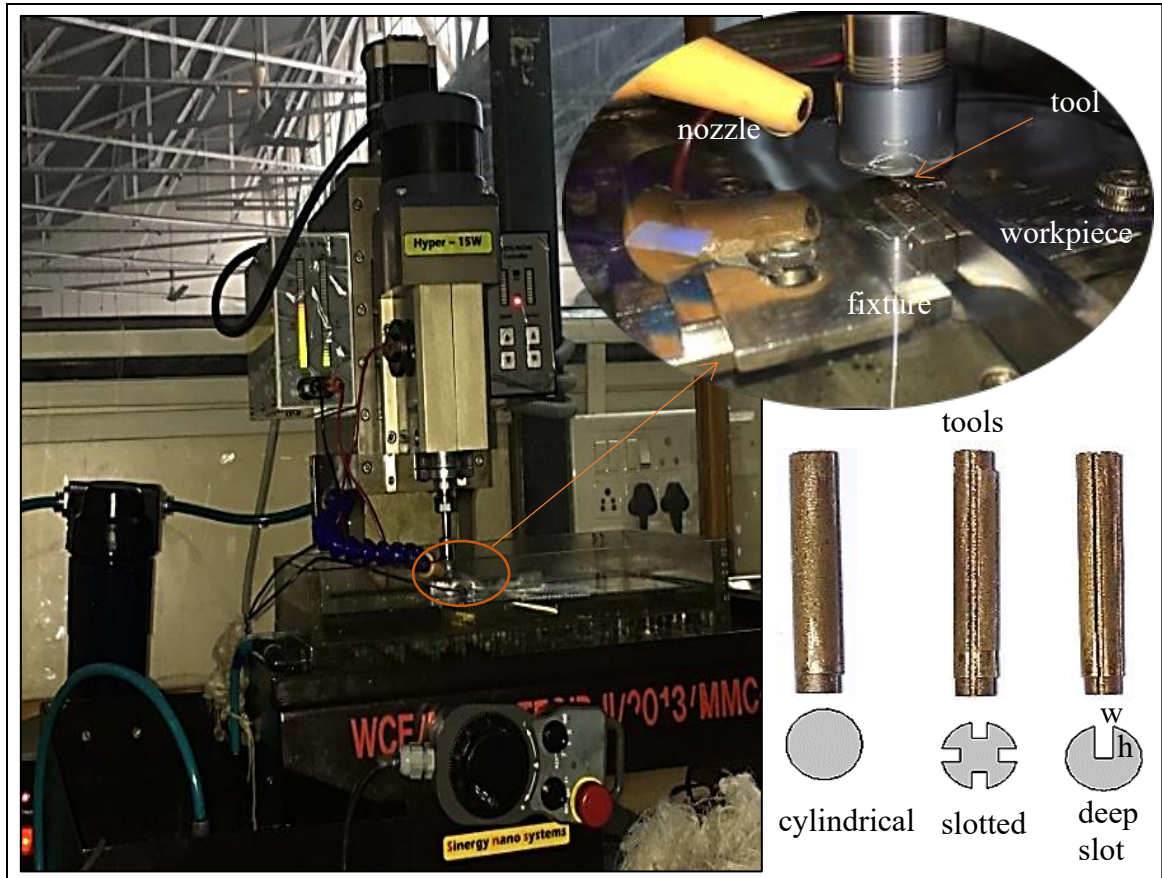


Figure 6.1 Setup using Hyper 15 machine and tools used for experimentation

Table 6.1 Parameters used and its specification

Sr. No.	Description	Values
1	Workpiece	EN31 (4 mm thick)
2	Tool	Copper (ϕ 2 mm)
3	Dielectric	EDM oil
4	Capacitance	10000 pF
5	Voltage	150 V
6	Speed	800 rpm
7	Feed	0.6 mm/min
8	Length of cut	1 mm
9	Depth of slot	1 mm

6.2.2. Effect of geometry of the tool

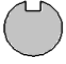
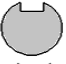







The objectives of the experimental work are to investigate the effect of geometric features of the tool on the machining performance. The geometric features include peripheral longitudinal slots on the cylindrical tools. The effect of slot size and the number of slots on the MRR and TWR is explored. The tool is of copper with a nominal diameter of 2 mm and length 12 mm. The slots of various dimensions are cut on the cylindrical tool using CNC controlled wire-EDM machine. The wire material to cut the slot is brass with a diameter of 0.25 mm. Three basic tool shapes considered for the study are cylindrical, slotted and deep slot as shown in Figure 6.1. The rotational speed of the tool is kept constant at 800 rpm and the depth of cut is 1 mm.

The slotted tool consists of 4 equispaced radial slots on the periphery, each of width 0.4 mm and height 0.5 mm. The deep slot tool consists of a single radial slot of width 0.4 mm and a height of 1 mm which is the radius of the tool. The effect of slot width and height on the removal rate is considered taking two different cases. In the first case, the slot width is varied by three values 0.5, 0.75 and 1 mm keeping the slot height constant at 0.4 mm. In the second case slot height is varied similarly by three values 0.5, 0.75 and 1 mm keeping the slot width constant at 0.4 mm as listed in Table 6.2.

The performance of tool geometric features on the machining performance is analyzed and compared with the cylindrical tool. The MRR and TWR for all the tools is listed in Table 6.3 and the comparison of three shapes of tool is given in Figure 6.2. The slotted tool reduces the total cross-sectional area by 25 % that of a cylindrical tool and the deep slot tool reduces the tool cross-sectional area by 15 % that of a cylindrical tool. The MRR and TWR are calculated by the conventional weighing method. The weight differences (in grams) of workpiece and tool before and after the machining are measured using precision balance. The least count of the precision balance used for weighing is 1 mg. It is observed that the slotted tool overperformed the cylindrical and deep slot tool. The radial slots on the periphery of the tool provide space for the debris to accumulate and eventually is flushed away due to tool rotation. This enhances the flushing of debris from the gap and improves the MRR. Due to effective flushing, the frequency of spark increases

in the gap which led to an increase in the TWR. In addition, due to the presence of slots the total area reduces increasing the TWR. This outcome of the experiment validates the simulation results where the maximum particles are removed from the gap in case of slotted tool with four slots.

Table 6.2 Various tool geometry

Tool No.	Tool dia. (mm)	No. of slots	Slot width (w) (mm)	Slot height (h) (mm)	Tool shape	Parameter
1	2	1	0.5	0.4		Effect of width
2	2	1	0.75	0.4		
3	2	1	1	0.4		
4	2	1	0.4	0.5		Effect of height
5	2	1	0.4	0.75		
6	2	1	0.4	1		
7	2	2	0.4	0.5		Effect of number of slots
8	2	3	0.4	0.5		
9	2	4	0.4	0.5		

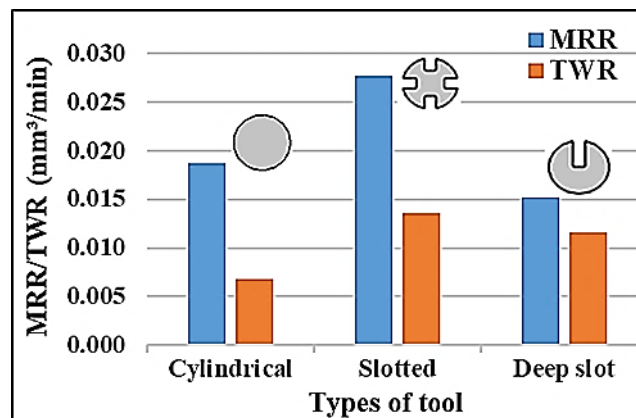


Figure 6.2 Effect of the tool shape on MRR and TWR

Table 6.3 Observation showing MRR and TWR for various tools

Sr. No	Tool geometry (w × h) (mm)	No. of Slots	Speed (rpm)	Reduction in Wt. of workpiece (gm)	Reduction in Wt. of tool (gm)	MRR (mm ³ /min)	TWR (mm ³ /min)	Time (min)
1	0.5 × 0.4	1	800	0.064	0.009	0.2505	0.0307	31.62
2	0.75 × 0.4	1	800	0.033	0.014	0.0329	0.0127	123.7
3	1 × 0.4	1	800	0.011	0.006	0.0211	0.0107	64.65
4	0.4 × 0.5	1	800	0.007	0.011	0.0108	0.0147	80.35
5	0.4 × 0.75	1	800	0.010	0.004	0.0274	0.0096	45.25
6	0.4 × 1	1	800	0.006	0.005	0.0152	0.0116	48.97
7	0.4 × 0.5	2	800	0.006	0.003	0.0122	0.0055	60.70
8	0.4 × 0.5	3	800	0.004	0.008	0.0109	0.0190	45.33
9	0.4 × 0.5	4	800	0.011	0.006	0.0277	0.0136	49.17
10	0.4 × 0.5	4	500	0.004	0.002	0.0156	0.0070	31.73
11	Cylindrical	-	800	0.005	0.002	0.0187	0.0068	33.03

6.2.3 Effect of number of slots

The machining performance enhanced with the slotted tool and hence further investigation is done to study the effect of the number of radial slots on the MRR and TWR. The number of slots considered are one, two, three, and four; further increasing the number of slots would reduce the strength of tool due to its small size. Figure 6.3 compares the MRR and TWR for a various number of radial slots on the periphery of the tool. It is observed that the tool with four slots has maximum MRR as compared to other tools. The MRR for all other tools having one, two and three slots are almost similar but has large variation in TWR. The tool wears with a faster rate for the tools with odd number of slots as compared to MRR. The MRR is higher than the TWR for the tools with even number of slots. The reason is sparking occurs on the workpiece surface where the IEG between the tool and the workpiece is less. However, in case of slotted tool, the probability of sparking in the slots is less. Slots affects the occurrence of sparking and it is not uniform along the surface of the tool. In addition, due to odd number of slots, the frequency of sparking varies resulting in uneven material removal from the tool near the slot which increases the TWR. The investigation is also carried out to study the effect of tool rotation speed on the

machining performance. The slotted tool with four slots which is the best option among all tools is selected with a tool speed of 500 and 800 rpm. The MRR and TWR is given in Figure 6.4 and it is observed that with the increase in the tool speed the MRR and TWR increases as expected. This is also observed in the simulation due to higher flushing caused due to high tool rotation speed.

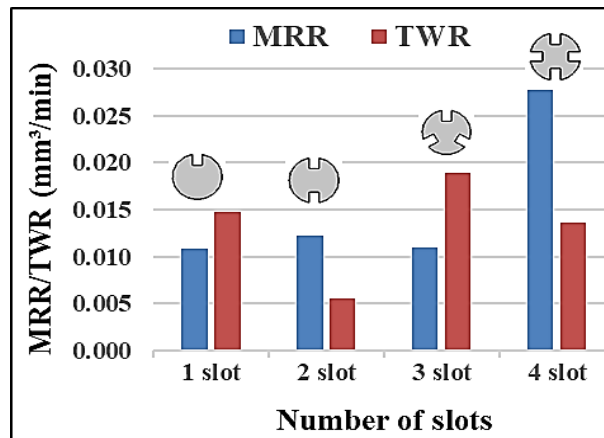


Figure 6.3 Effect of number of slots on MRR and TWR

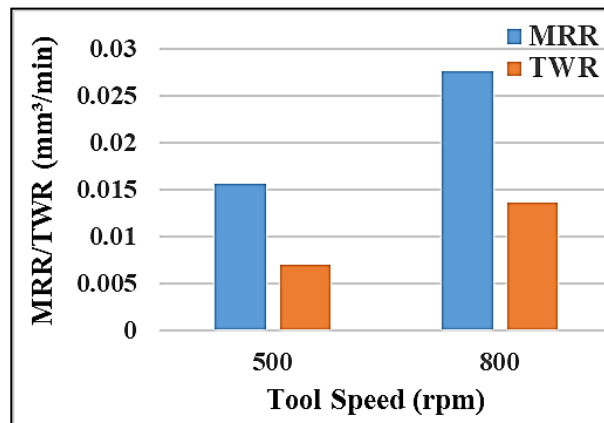


Figure 6.4 Effect of tool speed on MRR and TWR using slotted tool

6.2.4 Effect of slot width and height

The effect of slot width and height on the MRR and TWR is analyzed by varying the slot width keeping slot height constant and vice-versa. In both the cases, the cross-

sectional area of slot (width \times height) is constant and is 0.2, 0.3 and 0.4 mm² respectively. The effect of slot width and height on the MRR and TWR is represented in Figure 6.5. It is observed that the effect of a change in the width of the slot is considerable as compared to the height on the MRR and TWR. The change in the width of the slot decreases the active peripheral surface facing the workpiece which generates a spark and removes material. The optimum cross-sectional area of the slot is 0.2 mm² with slot width of 0.5 mm and height of 0.4 mm. With the same cross-sectional area interchanging the slot width and height decreases the MRR drastically.

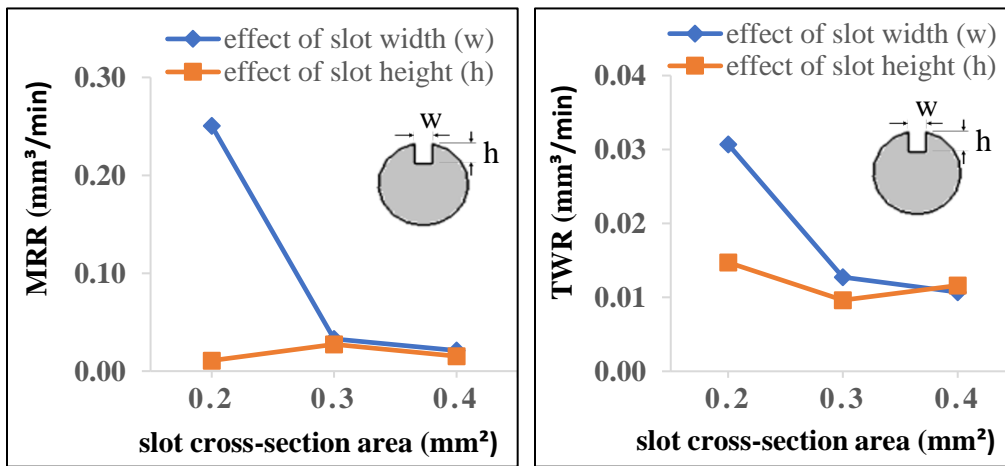


Figure 6.5 Effect of slot width and height on MRR and TWR

6.2.5 Microscopic study

The images of the cross-section of the tool before and after machining is taken using metallurgical microscope. This microscope is used for metallurgical inspection of metals, ceramics, and other materials. The maximum magnification capacity of the microscope is 1000 \times , but the images are taken at 40 \times magnification to cover the entire cross-sectional area of the tool. Figure 6.6 shows the microscopic images of different tools before and after machining. It is observed that tool wear is uniform along the circumferential surface in case of cylindrical and slotted tool with four slots. While in case of tools with one, two and three slots the wear is not uniform along the circumference. The observation of the tool after

machining revealed that the tool wears maximum near the slots. The tool with odd number of slots wears out at a faster rate as compared to the material removed.

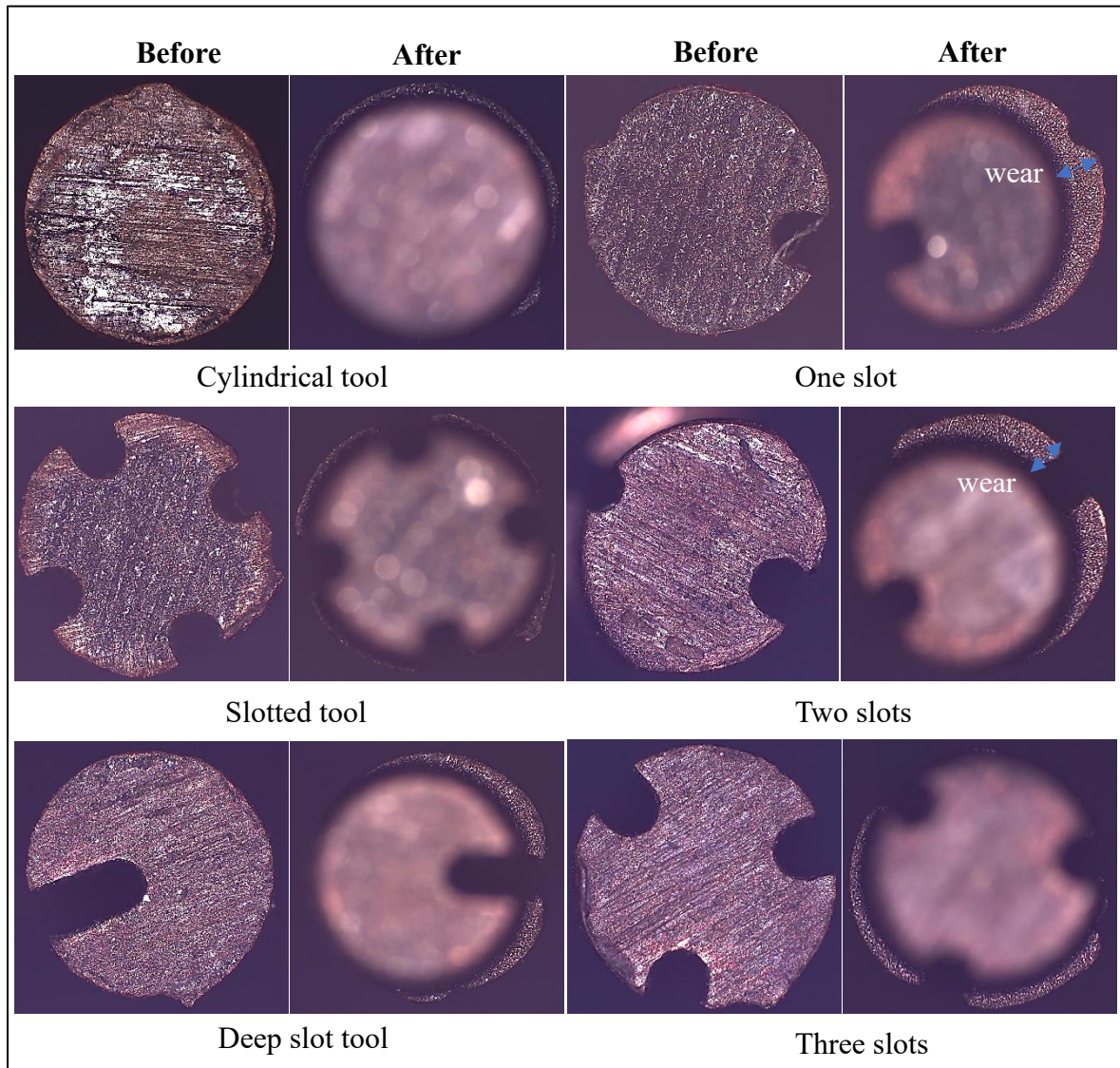
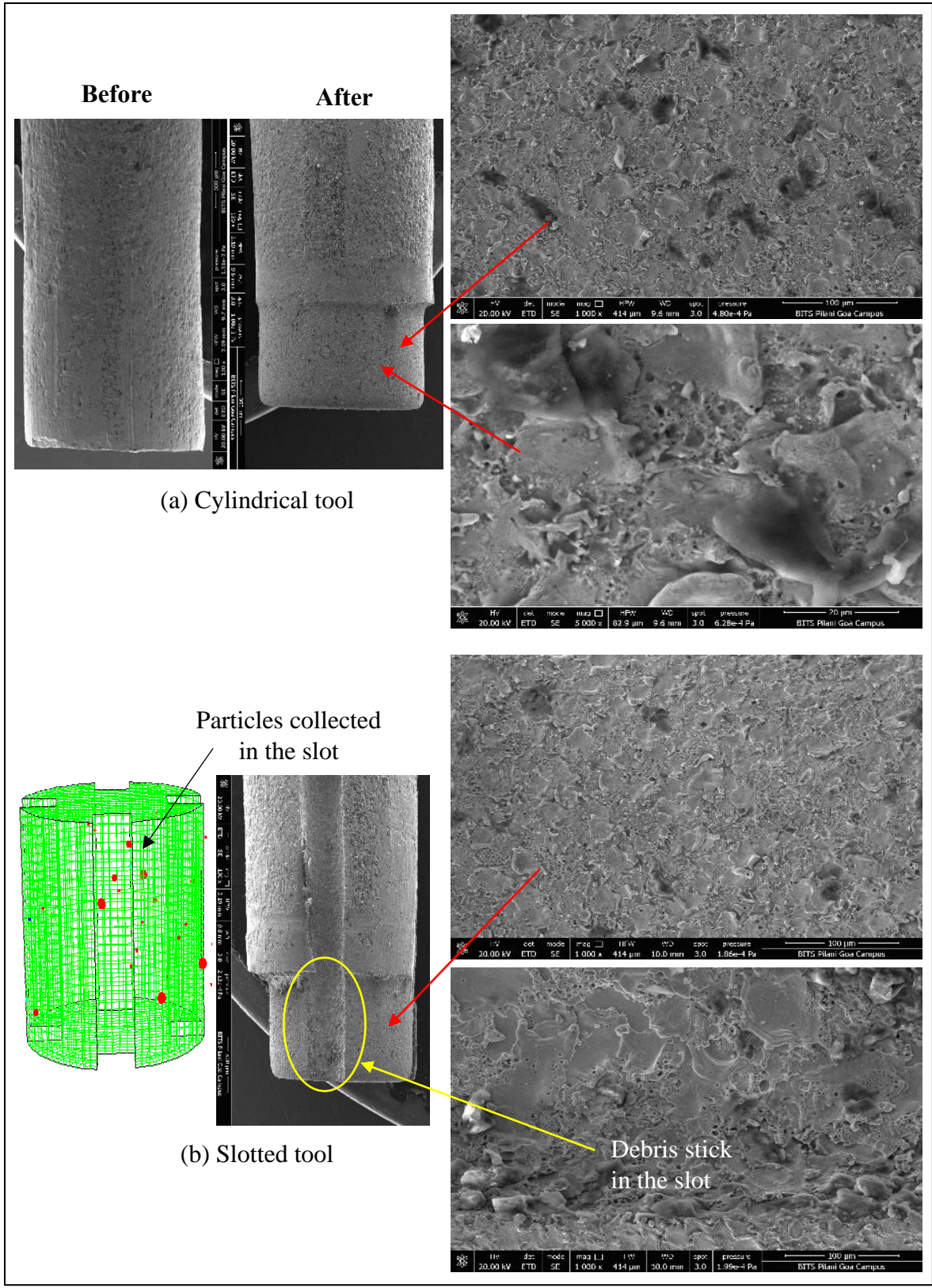


Figure 6.6 Microscopic images of the tool cross-section showing the wear of the tool

The scanning electron microscope (SEM) produces images by scanning the sample with a high-energy beam of electrons. A very high magnification of the order of 1,00,000 \times can be obtained. The microscopic images for the present study are taken at the magnification of 90 \times to 5000 \times . The SEM image showing shape and surface topography



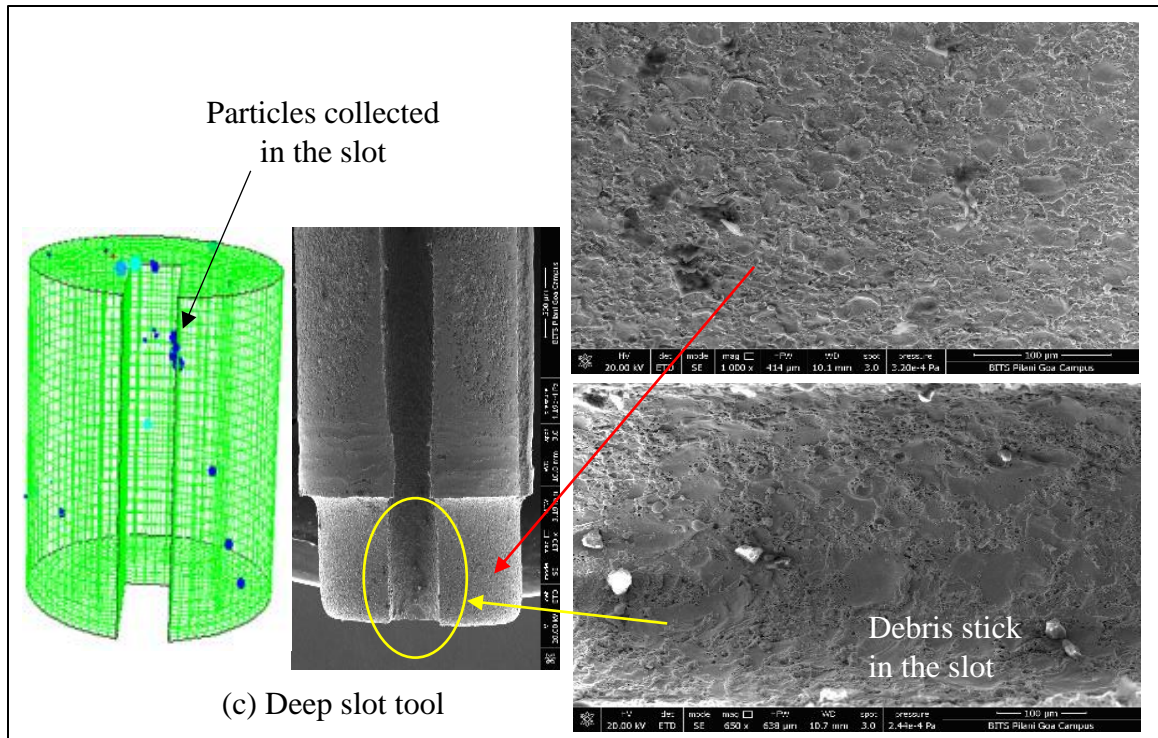


Figure 6.7 SEM micrograph morphology of various tools: (a) cylindrical, (b) slotted, and (c) deep slot tool

of the tool surface after machining is shown in Figure 6.7. The tool wear is clearly seen after machining the channel in one pass. The surface of the cylindrical tool is comparatively rough and many black spots are observed. This black spots may be due to the carbon emitted during machining and gets deposited on the tool surface. The surface of the deep slot and slotted tool is relatively smooth as compared to the cylindrical tool. Very few black spots are visible on the surface of the slotted tool and are smoother than the other two tool surface. This shows that the MRR is good using the slotted tool. The slot provided on the surface of the tool drags the debris from the IEG and collects it in the slot. When the temperature of the debris is very high and if it is unable to move out of the slot then it gets stick to the slot surface which is seen in Figure 6.7. The simulation of the particles ejected from the workpiece shows the accumulation of the particles in the slot similar to the experimental results.

The SEM image showing the surface topography of the machined channel using various tools is shown in Figure 6.8. Through channel is machined using single slot tool and it is visible in the figure that the channel is tapered. This is due to the wear of tool while machining the channel. It took nearly 2 hours to machine the channel and hence to reduce the time of machining the other channels are machined by traveling a distance of 1 mm in the workpiece. The comparison of the edges and surface of the channel machined by three different tools shows that the slotted tool overperformed the other two tools. The channel surface machined by slotted tools contain less unwanted particles and the edges are smooth as compared to the surface machined by cylindrical and deep slot tool. At a higher magnification scale, uniformly distributed particles are observed on the machined surface using the cylindrical and slotted tool. Similarly, the surface is smooth with only a few small pores visible. However, the surface machined using deep slot tool shows pores with large size and a greater number of pores. These pores may lead to the generation of crack. The surface is relatively rough and contains uneven size particles.

6.3. EXPERIMENTAL SETUP USING HIGH-SPEED CAMERA

The setup for experimentation includes work holding fixture, dielectric tank, and arrangement to supply the dielectric fluid. The experimental setup consisting of the tool, workpiece and the fixture is shown in Figure 6.9. The cylindrical tungsten electrode tool ($\text{\O} 500 \mu\text{m}$) is mounted rigidly on the spindle using the collet to avoid wobbling during rotation. A die material EN24 is chosen as a workpiece material (1.5 mm thick) which is clamped on the machine table using a fixture. The workpiece is ground on all faces to maintain flatness using a standard surface grinding machine. The dielectric used is conventional EDM oil and is supplied through a nozzle at the machining area to ensure continuous recirculation of the fluid. The entire setup is immersed in EDM oil in the tank. The dimension of the slot to be cut is length (1.5 mm), width (0.5 ± 0.1 mm), and depth (1 mm). The tool rotates and travels in a predefined straight path to cut a slot which is controlled by CNC servo control. Three levels of energy 50, 500, 2000 μJ and tool speed

of 100, 500, and 800 rpm is selected. The specifications of the tool and workpiece and the values of parameters used for experimentation are given in Table 6.4.

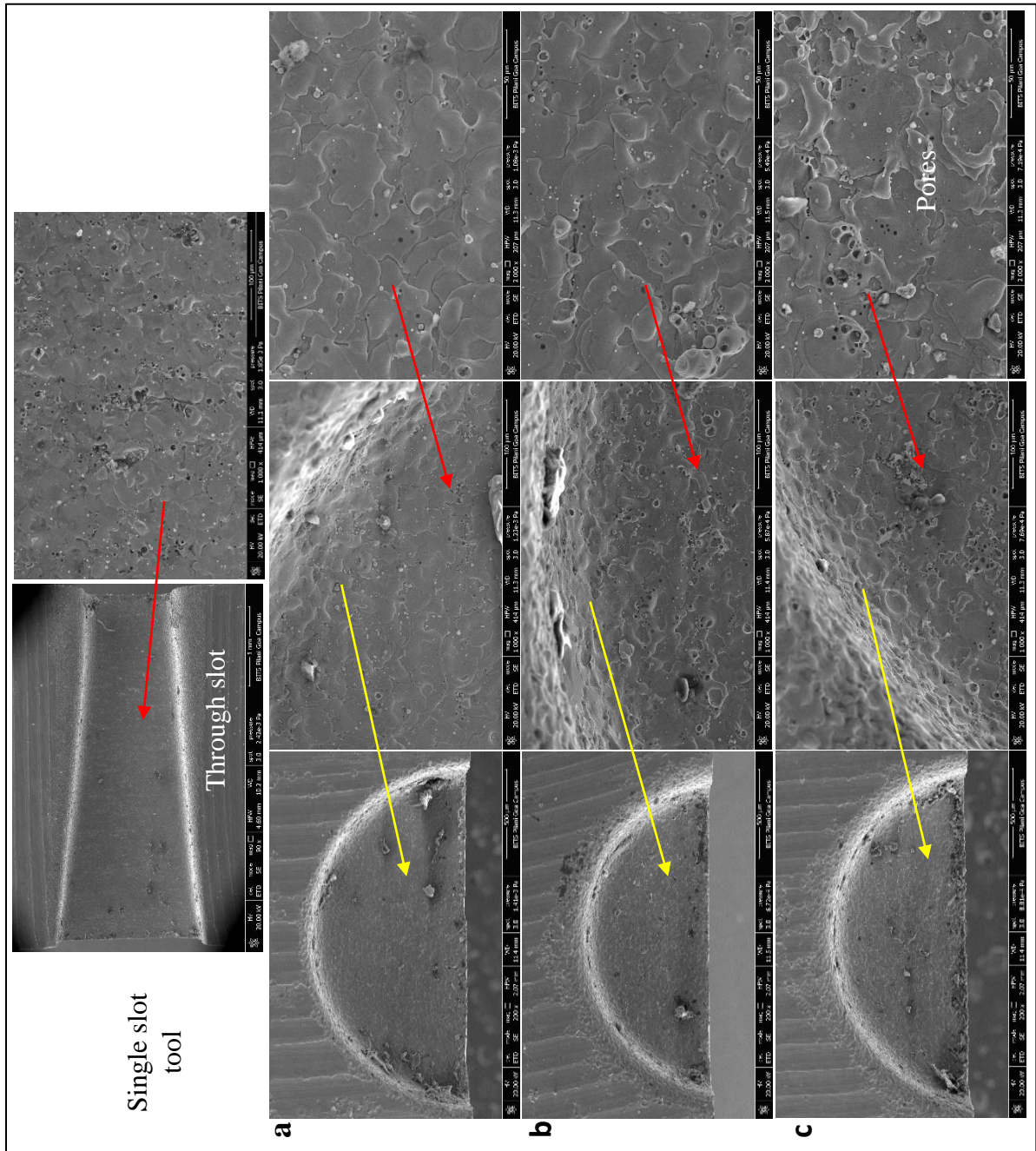


Figure 6.8 SEM micrograph morphology of channel surface machined using (a) cylindrical tool (b) slotted tool and (c) deep slot tool

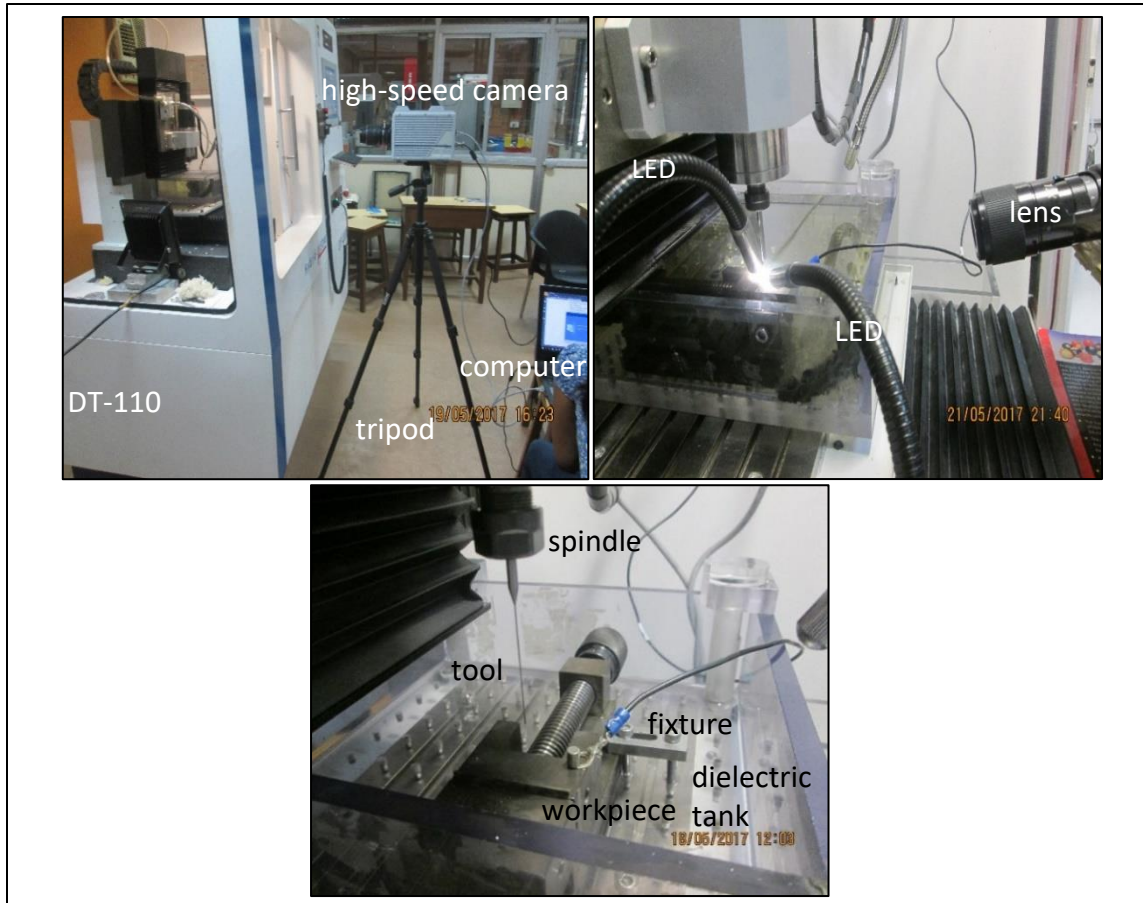


Figure 6.9 Experimental setup on DT-110 with phantom high-speed camera

Table 6.4 Process parameter for μ ED-milling and its specification

Sr. No.	Description	Values
1	Workpiece	EN 24 (1.5 mm thick), (+) polarity
2	Tool	Tungsten Carbide (\varnothing 500 μ m), (-) polarity
3	Dielectric	EDM oil
4	Capacitance	10, 100, 400 nF
5	Voltage	100 V
6	Energy	50, 500, 2000 μ J
7	Speed	100, 500, 800 rpm
8	Feed	0.6 mm/min
9	Depth of slot	1 mm

6.3.1. Experimental setup using Phantom high-speed camera

The initial experiments are performed using high-speed camera Phantom v8.002. The high-speed camera is mounted on the tripod and it is connected to the computer to store the video. The experimental setup is shown in Figure 6.9. The images are recorded with 1690 fps (frames per second) with a resolution of 1280×800 and exposure time of $590 \mu\text{s}$. The $12\times$ magnification lens is used to capture the micro details. The working distance is approximately 300 mm which is unable to reduce further due to machine structure and tripod holding the camera. The field of view (FOV) of camera is 5×5 mm. The 30W LED light source is used for illumination.

6.3.2. Experimental setup using pco. dimax high-speed camera

In the first attempt of pilot experiment the working distance of the lens and the object to be viewed was larger (300 mm). This was due to the large size of dielectric tank of the machine and the attachment of the tripod of camera. To reduce the working distance, the dielectric tank and the fixture to hold the workpiece was removed. A small setup was developed to reduce the working distance. A small glass beaker was used as a dielectric tank and the workpiece was firmly fixed in a slot provided on a copper block. The movement of copper block was eliminated by inserting suitable packing in the beaker. A large size camera stand was used so that camera with the lens can be moved near to the beaker. The experimental setup showing all the details is shown in Figure 6.10.

The high-speed camera used is pco. dimax HS4 high speed CMOS camera. It is able to capture images at a maximum frame rate of 46746 fps at a lower resolution of 320×200 . The storage memory required to save the data is large, hence images are captured at the highest resolution with 2277 fps. The lens used was Mitutoyo WD 43175717 with a $5\times$ magnification. The working distance was reduced to 30 mm. For illumination three LED lights of 18 and 24 W are used. The specifications of the high-speed video camera are given in Table 6.5.



Figure 6.10 Experimental setup on DT-110 with pco. dimax HS4 high speed camera

Table 6.5 Specifications of high-speed camera

Parameter	Specification
Make	pco. dimax HS4 high speed CMOS camera
Resolution (h × v)	2000 × 2000 pixels
Pixel size (h × v)	11 μm × 11 μm
Exposure /shutter time	1.5 μs to 40 ms
2000 × 2000 pixels	2277 fps (min.)
320 × 200 pixels	46746 fps (max.)

6.4 HIGH-SPEED IMAGES

6.4.1 Sparking

The high-speed images of the spark are shown in Figure 6.11. In μ ED-milling due to high rotation speed of the tool, spark occurs all around the periphery of the tool. Due to this, the ring like structure of the spark is observed in Figure 6.11 (a) which is unique in μ ED-milling. This is not observed in die-sink EDM as the tool is stationary. The reflection of the tool is observed in the dielectric fluid. Further' in order to study the behavior of the spark, the spark is generated along the workpiece top surface and the tip of the tool. The cylindrical tip of the tool gets converted into conical shape after machining of a μ channel due to wear. This conical shape tool is used to generate spark along the top surface of the workpiece. Figure 6.11 (b) shows the spark for different input energies. It is observed that the spark is elliptical and uniform at lower energy of 50 μ J. With the increase in energy to 500 and 2000 μ J the spark is larger and covers the side face of the tool. At tool speed of 500 rpm, the size of spark is calculated for different energy levels. The size of spark calculated is 35, 50 and 75 μ m for input energy of 50, 500 and 2000 μ J respectively. The size of spark is approximately equal to the IEG. The calculated IEG size is in close resemblance with the IEG size used for CFD simulation. The limitation of simulation was it was not able to model spark generated in the gap.

The effect of input energy on the spark behavior is studied at a constant tool speed of 800 rpm as shown in Figure 6.12. The images are taken at a frame rate of 2277 fps so each frame is captured at 0.4 ms. At a high energy of 2000 μ J, the spark with larger size is observed at the bottom and periphery of the tool. When the spark ceases, bubbles of larger size are formed around the tool. These bubbles entrap carbon and debris particles and due to density difference, it travels in upward direction and eventually burst. The bursting causes black layer of carbon particles to be expelled from the zone. This process continues after every spark and is responsible to remove the machining byproducts from the gap. The clear image of debris particles getting expelled from the crater is not visible due to constraint of the available lens. It requires microscopic lens to capture micro and nano

debris particles. At lower energy conditions, the size of spark and bubbles generated decreases due to which the carbon layer is not visible in Figure 6.12.

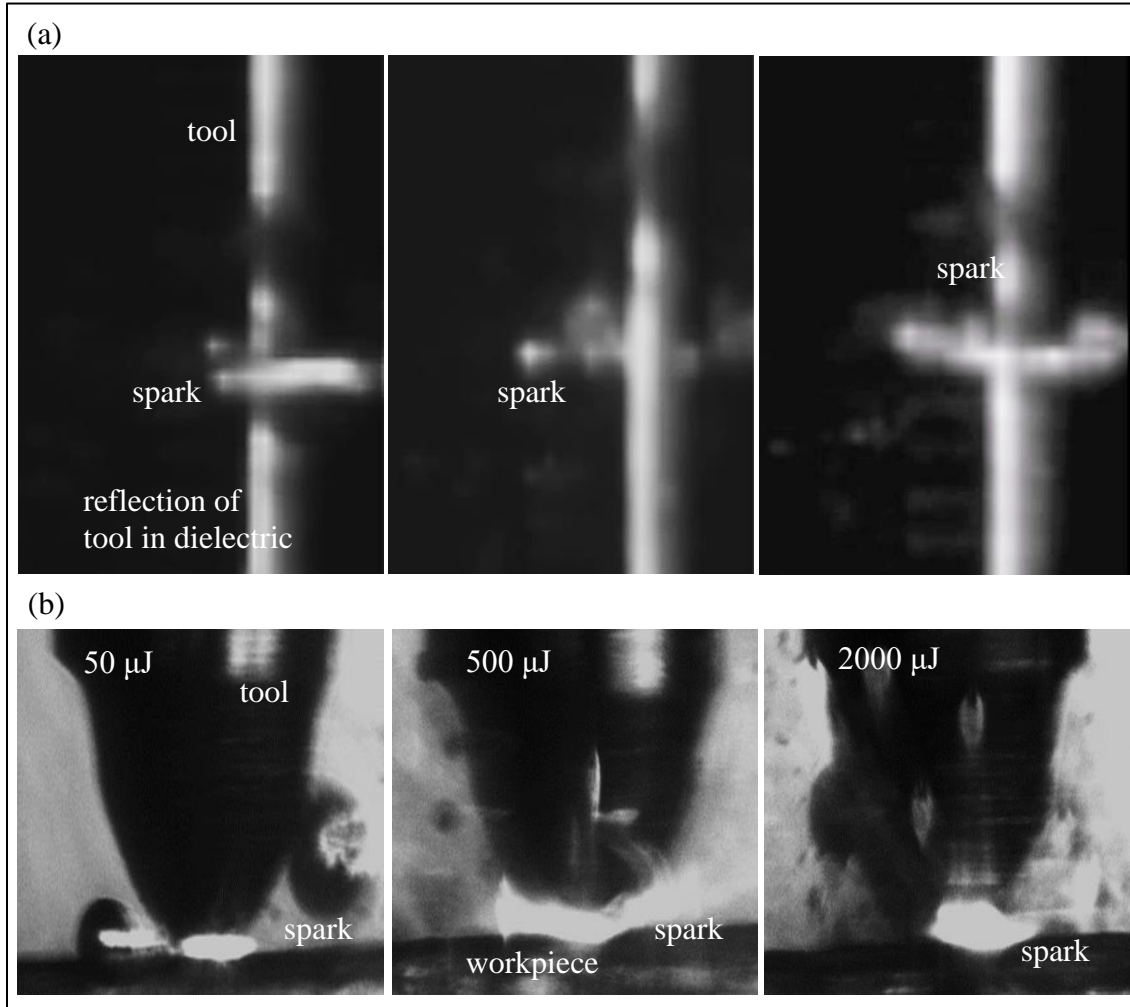


Figure 6.11 High-speed images of spark along (a) periphery and (b) tip of the tool

6.4.2 Dielectric flow

The velocity of the dielectric fluid in the IEG is the major reason to remove the debris from the gap. It is difficult to measure the velocity of dielectric at the IEG of size less than 50 μm. Hence the high-speed images of the sparking zone are used to find the velocity of the dielectric fluid. Table 6.6 shows the dielectric velocity in the IEG at various tool speed. The size of the bubble is calculated and the distance travelled by the bubble for

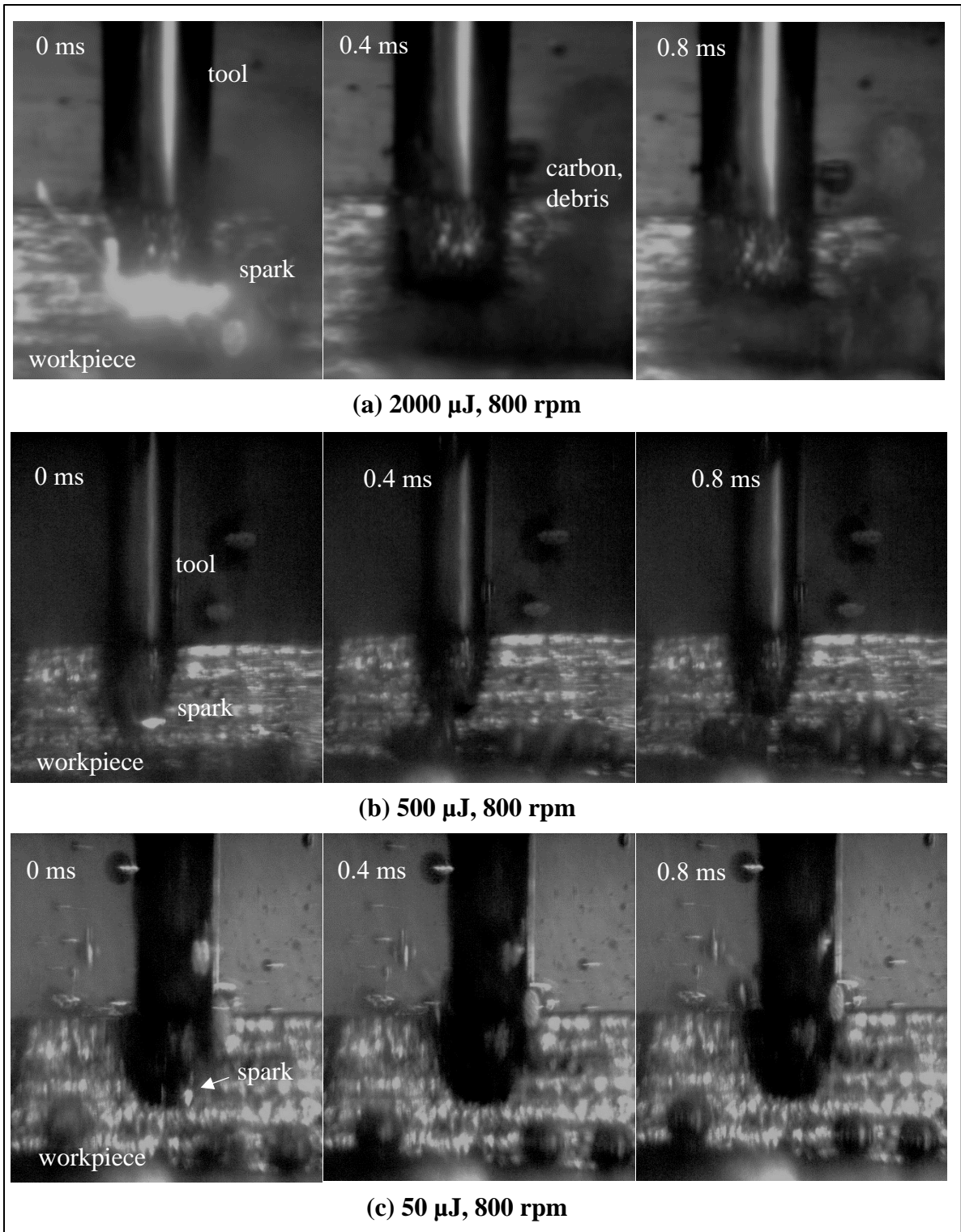


Figure 6.12 High-speed images of spark and bubbles generated for different input energies

specific time frames are used to find the velocity of the bubble. This velocity is approximately equal to the velocity of dielectric. It is found that at tool speed of 100, 500 and 800 rpm the velocity of the dielectric fluid is 0.4, 1.23 and 1.99 cm/s respectively as shown in table. These velocity values are close to the values found using CFD simulation.

The flow-field in the μ channel obtained using simulation is validated using two different methods. The experimental SEM micrographs of the machined μ channel shown in Figure 6.13 (a) gives the clear picture of the flow pattern, deposition point and vortex at the back of the tool. This is similar to the pattern observed in the simulation as represented in Figure 6.13 (b). However, as the SEM images are taken after the machining, the in-process images of flow behavior are captured using high-speed camera. The vortex and the fluid flow near the tool are clearly seen in the high-speed video camera images of the micro tool taken at high magnification and frame rates as shown in Figure 6.14. All the method shows the similar nature of dielectric flow around the tool.

Table 6.6 Dielectric velocity at IEG

Sr. No.	Tool speed (rpm)	Bubble dia. (μm)	Distance traveled (μm)	Time (ms)	Velocity (cm/s)
1	100	192	72	18	0.4
2	500	250	260	20.8	1.23
3	800	237	112	5.6	1.99

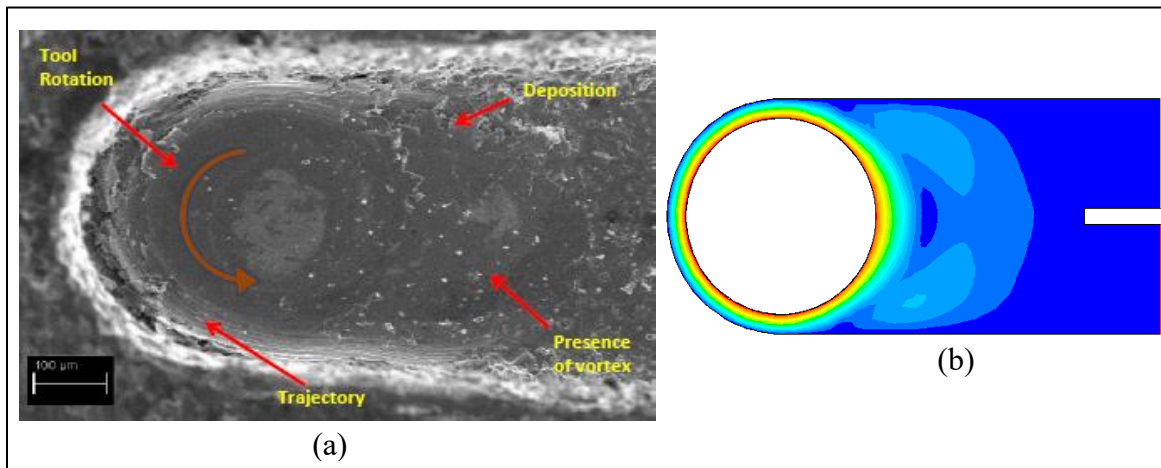


Figure 6.13 (a) SEM image showing trajectory, deposition point and (b) Velocity contour

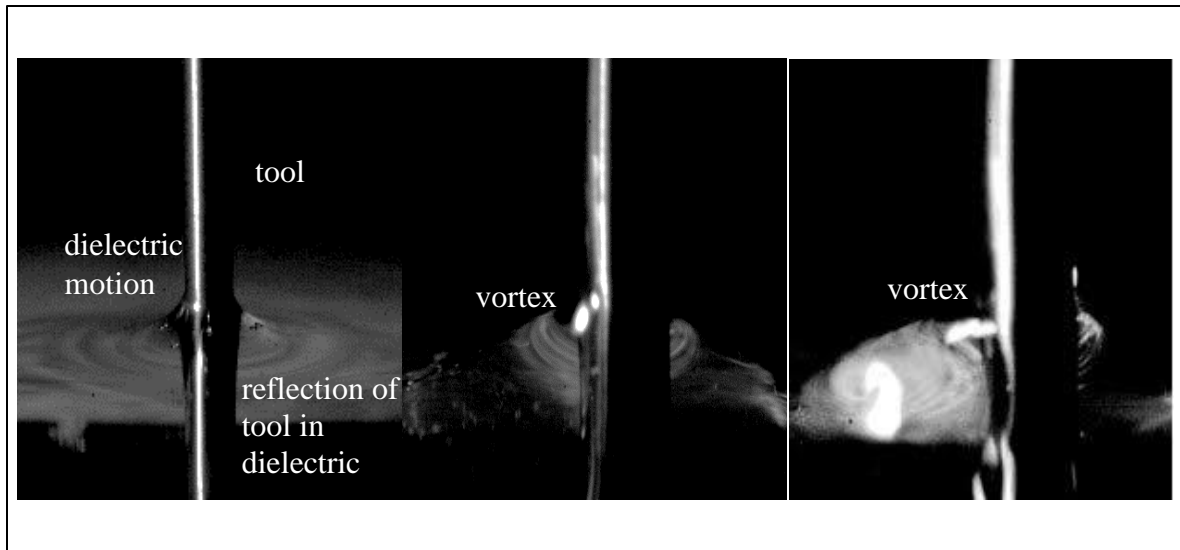


Figure 6.14 High-speed images showing the dielectric flow and vortex at the back of the tool

6.4.3 Debris particles

The SEM micrographs are obtained for each channel which shows the 2D surface behavior of machining. The results of the 2D simulation are verified with a micrograph of the machined μ channel. Figure 6.15 (a) shows SE micrograph of debris on the work surface at various conditions. It is evident from the figure that debris particles are spherical in shape with various sizes that attach to work surface. The size of the debris is approximately equal to the size of the crater. The particle size used in the simulation is similar to the size of debris observed in SEM image. Rotation of the tool increases disturbance in the gap and probability of simultaneous sparking. The molten metal ejected from the crater gets split into fine particles due to high tool speed. The kinetic energy of the debris is reduced by the viscous dielectric fluid. Further rotation of tool exerts centrifugal force on the debris and pushes it towards the stationary work surface. Figure 6.15 (b) shows the tool and work surface which shows that the work surface is relatively rough than the tool surface due to redeposition of debris on the work surface. The amount of redeposition is less on the tool surface due to rotating tool which is inherent part of μ ED-milling process. Figure 6.15 (c) shows the deposition on the walls of the μ channel. For the similar area on the side walls, it is observed that deposition rate is 30% more on one side of the μ channel. Hence, μ channel

appears to be slightly tapered. This result is similar to the simulation results where the accumulation of particles is observed on one surface of the workpiece. It is observed that the width of the vortex along the tool travel is 0.16 mm on SEM image and 0.202 mm with simulation results. The trajectory of the debris movement is mainly governed by the direction of tool rotation. The length of the trajectory of the particle is 1.25 mm on SEM image, and it is 1.8 mm using simulation results. The size of the vortex and the distance travelled by the particle using simulation and experimental method is given in Table 6.7. The simulation results are reasonably in accordance with experimental micrographs.

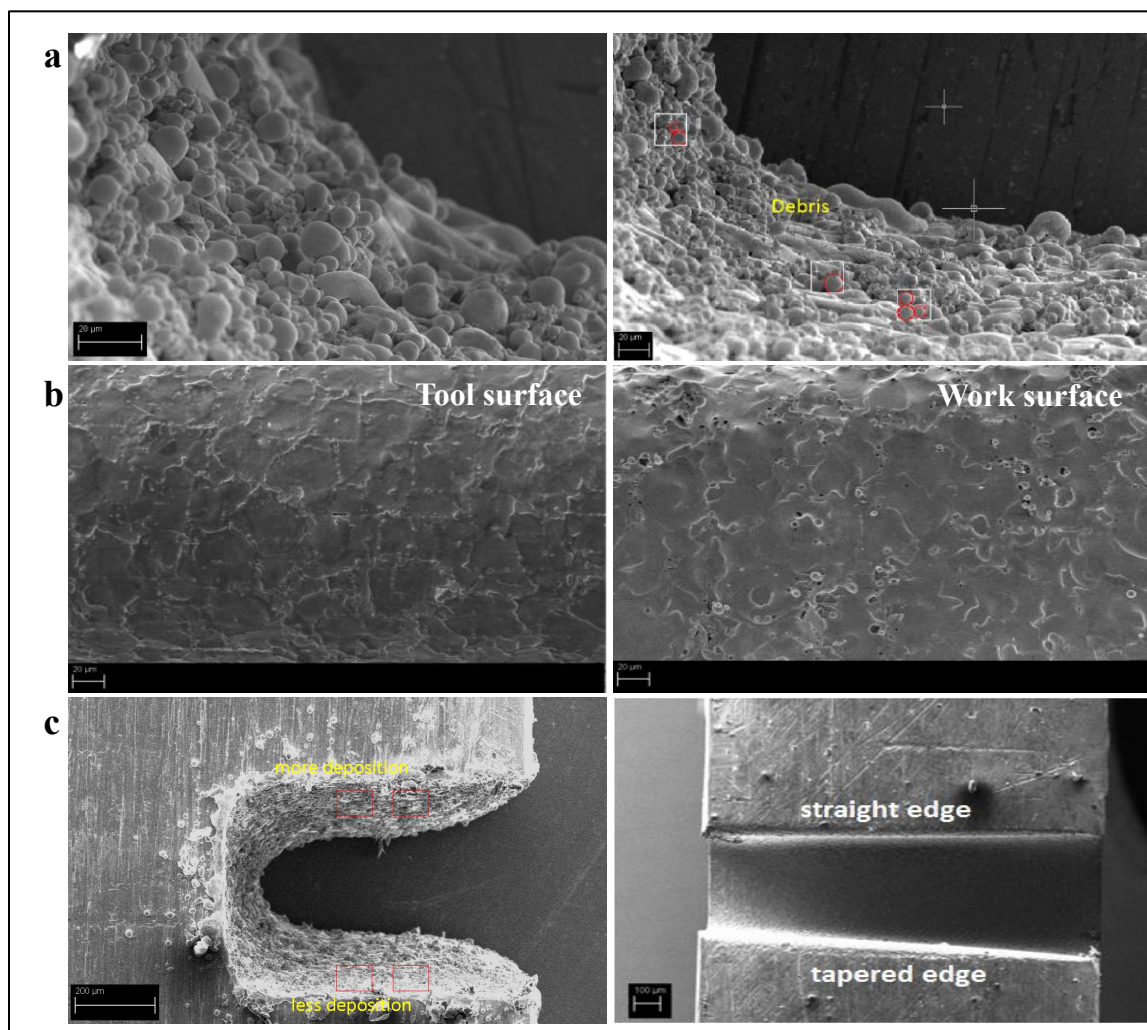


Figure 6.15 SEM images showing (a) debris particles at 2000 μJ , 800 rpm (b) tool and work surface at 500 μJ , 500 rpm (c) taper in the $\mu\text{channel}$

Table 6.7 Vortex size and distance travelled by particles

Analysis Technique	Tool Dia. (mm)	Channel width (mm)	Distance travelled in one rotation (mm)	Number of particle rotations	Total distance travelled (mm)	Vortex height (mm)	Vortex width (mm)
CFD	0.5	0.6	1.8	6	10.8	0.33	0.26
SEM	0.5	0.6	1.25	1	1.25	0.27	0.23

6.5. SUMMARY

The experimental study explores the suitability of using slotted tools in comparison to the cylindrical tools towards enhancing the MRR. The flushing efficiency of slotted tools with four slots found most effective and is verified experimentally. The reduction of tool cross-section area by 25% increased the MRR by 150% as compared to the cylindrical tool. The effect of slot width as compared to slot height is more on the MRR and TWR. The surface topography of the cylindrical tool shows black spots and relatively high surface roughness as compared to a slotted tool which shows the inability of the tool to remove the byproducts of the machining. The machined channel using slotted tool shows a smooth surface with uniformly distributed particles. These advantages of the slotted tool make it appropriate to be used for ED milling.

The experiments using high-speed camera is used to capture the spark, dielectric flow and debris in the IEG. The high-speed images of spark show that the IEG formed between the tool and workpiece is in close resemblance with the gap width selected for simulation. The size of spark increases with the increase in the input energy and it is continuous along the bottom and side surface of the tool. The velocity of the dielectric found at the IEG using high-speed images matches the simulation results. The vortex at the back of the rotating tool is clearly observed. Due to practical difficulty, debris are not visible in the images but the SEM micrograph shows spherical debris deposited on the workpiece surface.